Iranian Journal of Fuzzy Systems

Volume 19, Number 5, (2022), pp. 111-129

Original paper

University of Sistan and Baluchestan

Supervisory adaptive interval type-2 fuzzy sliding mode control for planar cable-driven parallel robots using Grasshopper optimization

Mh. Aghaseyedabdollah[1], M. Abedi[2] and M. Pourgholi[3]

[1,2,3] *Department of Electrical Engineering, Shahid Beheshti University, Tehran, Iran*

M.aghaseyedabdollah@mail.sbu.ac.ir, Mo_abedi@sbu.ac.ir, M_pourgholi@sbu.ac.ir

Abstract

Design of an adaptive supervisory fuzzy sliding mode control for a planar cable-driven parallel robot is aided in this paper. The fuzzy logic controller is proposed to generate the switching control signal without occurring the chattering problem. For this purpose, an adaptive mechanism is suggested for online tuning of the output gain of the fuzzy sliding mode controller. Moreover, for better tracking, a supervisory control system is considered for online tuning of the PID sliding surface gains. The Grasshopper Optimization Algorithm is suggested for optimization of the membership functions selected for the fuzzy sliding surface. The stability proof of the closed-loop system is derived by using the Lyapunov stability theorem. Simulation results are reported to show the merits of the proposed controller on reduced chatter, and system robustness against parameter uncertainty, load disturbance, and nonlinearities.

Keywords: Cable-driven parallel robot, internal force, sliding mode, interval type-2 fuzzy system, adaptive, supervisory control, chattering, the grasshopper optimization algorithm.

1 Introduction

Cable Driven Parallel Robot (CDPR) is a type of robot manipulator which has an end-effector driven by several parallel cables, as substitutes for rigid links. They have found useful applications in practical cases such as high-speed utilization [14], the rescue missions in dangerous environments [19], transportation of the heavy materials [7], and medical rehabilitation equipment [32]. CDPRs have been sorted into two types, under-constrained and fully-constrained [6, 20]. In the fully constrained cable robots, which is considered in this work, the number of robot degrees of freedom is less than the number of actuators [11]. Extra cables can provide larger workspaces and optimized performance for cable robots. New challenges have been occurred in cable robots by replacing rigid links with cables. It should be noted that only tensile forces can be generated by the cables that cannot push anything and just be used to pull objects. Therefore, the controller should be designed in such a way that the cables remain in tension at the whole workspace. Several conventional algorithms for control of CDPRs such as predictive control [13], fuzzy plus PI control [8], linear quadratic optimal controller [10], and Lyapunov-based methods [25], have been designed. In another research, for a 3DOF planar cable-driven parallel robot, an LQ optimal controller is proposed [1]. In [18],$H\infty$ control for the cable-driven parallel robot has been offered. The authors in [19], suggested a robust PID control for the practical fully-constrained cable robots. In [17], the robust PD control considering uncertain Jacobian matrix for the parallel-wire-driven system has been introduced. In another research, an adaptive control method with uncertainties in kinematic and dynamic parameters for the CDPR is suggested [4]. In [15], a robust dynamic sliding mode control method was suggested for a deployable cable-driven robot. It should be noted that the feedback gains of the switching terms should be chosen large enough to reduce the effect of uncertainties and guarantee the system stability. However, the high values of the feedback gains cause a chattering problem, which is very destructive to the system. To solve the mentioned problem, an idea has been suggested in [2, 30] combining the fuzzy control scheme with the sliding mode

Corresponding Author: M. Abedi

Received: November 2021; Revised: May 2022; Accepted: July 2022.

https://doi.org/10.22111/IJFS.2022.7160

control (SMC), and the system robustness is guaranteed despite decreasing the chattering effects. Authors in [35] have used fuzzy SMC (FSMC) for a complex robot system in the presence of exogenous disturbances. In [24], an adaptive fuzzy sliding mode control (AFSMC) method for force/position control in Stewart manipulator (SM) has been reported. In another research [27] for 2 DOF robot manipulators, supervisory fuzzy logic control (SFLC) has been utilized for online tuning of the output gain of FSMC and the results denote the considerable reduction of the chattering effects that are robust against parameter uncertainties.

Recently, type-2 fuzzy logic controller has attracted many attentions in compared with type-1 fuzzy logic control. In interval type-2 fuzzy logic control (IT2-FLC), the membership functions (MFs) have interval fuzzy form, and an extra degree of freedom is provided by the footprint of uncertainty (FOU). Type-2 fuzzy logic controller suggests good abilities to handle linguistic uncertainties by modeling the unreliability of the information, and in comparisons with the type-1 fuzzy system has better performance in the presence of nonlinearities and uncertainties. Hybrid methods such as combinations of type-2 fuzzy logic control with sliding mode have the advantages of both controllers which have attracted the attention of researchers. A type-2 fuzzy sliding mode control scheme was suggested in [3], for mobile robot navigation. In [29], sliding mode control with an interval type-2 fuzzy system has been introduced for synchronization of two different chaotic systems in the presence of disturbances and, uncertain system modeling. The type-2 fuzzy logic controller is used for chattering reduction, and improving the robustness of the reaching phase part. An IT-2FSMC is presented in [12] for a robot manipulator with external disturbances. In [33], for the accurate trajectory of a machining tool application, an interval type-2 fuzzy proportional-integral sliding mode control is presented on the XY motion stage. In [23], a robust adaptive interval type-2 fuzzy sliding mode controller is suggested for (MIMO) nonlinear systems with unknown disturbances and unmodeled dynamics. A novel robust adaptive-backstepping-recurrent-fuzzy-wavelet-neural-networks controller (ABRFWNNs) was proposed in [28].

Due to this fact that the fuzzy logic control design is based on trial and error, it will be difficult to find the best membership functions and fuzzy rules that may not lead to optimal performance. In recent years in order to have an optimized solution or near-optimal fuzzy rules, using the optimization algorithms for the membership function selection is offered. There are various methods to regulate the parameters of FLC. Between them, the metaheuristic algorithm methods are strong tools and capable of solving controller parameters design problems. In recent years the optimization method such as Newton Method [9] and population-based algorithms due to inspiration from nature, have high popularity which they are mimic behave of living creatures. Some swarm intelligence optimization techniques for optimization of fuzzy parameters are suggested in recent years such as Gray Wolf Optimization (GWO) [32], Whale Optimization Algorithm (WOA) [26], Artificial Bee Colony (ABC) [34], particle swarm optimization[6] . The Grasshopper Optimization Algorithm (GOA) [31] is a powerful metaheuristic algorithm which has attracted a lot of attention in recent years. GOA is a population-based algorithm and in the category of swarmed intelligence optimization methods. Moreover, GOA has less computational complexity in comparison to lots of optimization methods. In [21], for a 4 DOF quadrotor, a fuzzy adaptive robust PID controller is suggested. The optimized fuzzy system by GOA is used for tuning the gains of sliding surfaces in the presence of uncertainties and disturbances which causes improving control performance. It should be noted that few cases from using GOA for optimization of fuzzy systems have been developed in recent years while this algorithm has some advantages mentioned above. According to this topic, it is expected that the researchers use GOA for optimization of fuzzy systems in different control applications in the future.

In this paper, design of a supervisory adaptive interval type-2 fuzzy sliding mode control (SAIT-2FSMC) with the fuzzy PID sliding surface is investigated for a planar cable-driven parallel robot. The interval type-2 fuzzy tuning methods have been incorporated in the suggested controller to reduce the chattering effect and improve the system robustness against parameter uncertainty, nonlinearities, and load disturbance. By using the supervisory interval type-2 fuzzy gain scheduling for online tuning of PID sliding surface gains, it will be shown that the proposed controller has less tracking error and achieves better performance than the sliding mode control (SMC), interval type-2 fuzzy sliding mode control (IT-2FSMC), and adaptive interval type-2 fuzzy sliding mode (AIT-2FSMC) with constant gains. Also, the Grasshopper Optimization Algorithm (GOA) is used for the optimization of the membership functions of the interval type-2 fuzzy sliding surface system. The system stability is proved by using the Lyapunov theorem. The paper contributions are summarized as follows:

1) An intelligent robust method is developed for cable driven parallel robots in such a way that major structural challenges in these vehicles are considered. For this purpose, the proposed algorithm is combined with the internal force concept to produce positive forces that keep the cables in tension style.

2) The proposed algorithm is developed in such a way that the effects of most different disturbing factors on cable robots such as parametric uncertainties in the inertia matrix of robots and actuators, geometric structure of robots such as pulleys, Coriolis effects, and unknown models due to viscous and Coulomb frictions are considered.

3) An adaptive fuzzy structure is suggested to avoid the inherent chattering of the sliding mode controllers. Therefore, while achieving the asymptotic stability, a feasible control output is created.

4) Due to high nonlinearity of dynamical equations of cable robots, a sliding surface is introduced that its gains are adjusted adaptively. For this purpose, a supervisory fuzzy system for online tuning of PID sliding surface gains is replaced with the constant gains counterparts.
5) To make the best choice for parameters of the fuzzy membership functions, the Grasshopper Optimization Algorithm (GOA) is used to optimally adjust the mentioned parameters.
The rest of this paper is organized as follows: Preliminaries and definitions are described in Section 2. Section 3 describes the kinematic and dynamic modeling of a planar cable-driven parallel robot. In Section 4, suggested controllers for robust control of the robot are presented. The simulation results of the offered control method applied to a planar cable-driven parallel robot have been included in Section 5. Finally, conclusion is in Section 6.

2 Interval type-2 fuzzy logic systems

In interval type 2 fuzzy logic control (IT-2FLC), the membership functions (MFs) are interval fuzzy form while in type-1 fuzzy set the grade of membership functions are crisp. The general IT-2FLC structure is illustrated in Figure1. An IT-2FLC structure consists of five parts: a fuzzifier, a defuzzifier, an inference engine, fuzzy rules, and a type-reducer. A type-2 fuzzy system, shown as $\tilde{A}$ characterized by $\mu_{\tilde{A}}(x,\nu)$ which is a type-2 membership function defined as follows:

$$\tilde{A} = \{(x,u), \mu_{\tilde{A}}(x,\nu) : \forall x \in X, \nu \in J_x \subseteq [0,1]\}, \tag{1}$$

where $x \in X$, $\nu \in J_x \subseteq [0,1]$, $0 \leq \mu_{\tilde{A}}(x,\nu) \leq 1$ and $\tilde{A}$ is characterized as follows:

$$\tilde{A} = \int_{x\in X} \int_{u\in J_x} \frac{\mu_{\tilde{A}}(x,\nu)}{(x,u)} \qquad J_x \subseteq [0,1]. \tag{2}$$

Here $\iint$ denotes the union operation, J_x is the primary MF and $\mu_{\tilde{A}}(x,\nu)$ is the secondary MF amplitude. The FOU in type-2 fuzzy set $\tilde{A}$ has referred to a region bounded by a lower MF and an upper MF which are represented as $\underline{\mu}_{\tilde{A}}(x), \bar{\mu}_{\tilde{A}}(x)$, respectively. According to [21], the interval type-2 fuzzy system is developed by considering $\mu_{\tilde{A}}(x,\nu) = 1$ that $\tilde{A}$ can be represented as follows:

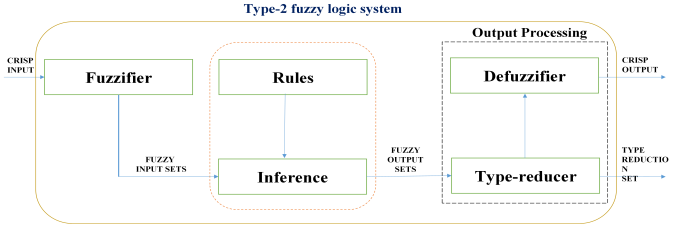


Figure 1: The general structure of type-2 fuzzy logic system

$$\tilde{A} = \int_{x\in X} \int_{u\in Jx} \frac{1}{(x,u)} = \int_{x\in X} \frac{\left[\int_{u\in Jx\subseteq[0,1]} \frac{1}{u}\right]}{x}. \tag{3}$$

IT-2FLC rules are similar to T1FLC, so there are N rules for the T2FLC with n inputs and m outputs that $x_1 \in X_1, ..., x_n \in X_n$ *and* $y \in Y$. A typical rule structure for $n = 1, ..., N$ can be expressed as follows:

$$R^n : \text{If } x_1 \text{ is } \tilde{X}_1^n \text{ and } ... \ x_m \text{ is } \tilde{X}_m^n \text{ , then } y \text{ is } \tilde{Y}^n. \tag{4}$$

In an interval type-2 fuzzy logic system, the general calculations that commonly consist of steps for generating a crisp output is needed. These steps are expressed as:
1. The fuzzifier part maps the crisp input $x = (x_1, ..., x_m)$ into IT-2FS.
2. By considering the inference mechanism and rule base, the firing interval $F^n(x)$ is calculated as:

$$F^n(x) = [\underline{f}^n, \bar{f}^n], n \in [N], \tag{5}$$

where

$$\underline{f}^n = [\underline{\mu}_{\bar{X}_1^n}(x_1) \times ... \times \underline{\mu}_{\bar{X}_m^n}(x_m)],$$

$$\bar{f}^n = [\bar{\mu}_{\bar{X}_1^n}(x_1) \times ... \times \bar{\mu}_{\bar{X}_m^n}(x_m)]. \tag{6}$$

Here $\times$ shows the product t-norm.
3. In this step, the type reducer is used in order to change the type-2 fuzzy output sets to type-1 fuzzy sets. Center-of-set (COS) is widely used for the type reduction method that is also considered in this paper and expressed as follows:

$$Y_{\cos}(x) = \bigcup_{\substack{f^n \in F^n(x) \\ y^n \in f^n}} \frac{\sum_{n=1}^{N} y^n f^n}{\sum_{n=1}^{N} f^n} = [y_l, y_r]. \tag{7}$$

Where consisted of its right and left points as y_r and y_l as:

$$y_r = \frac{\sum_{n=1}^{R} \bar{y}^n \underline{f}^n + \sum_{n=R+1}^{N} \bar{y}^n \bar{f}^n}{\sum_{n=1}^{N} \underline{f}^n + \sum_{n=R+1}^{N} \underline{f}^n}. \tag{8}$$

$$y_l = \frac{\sum_{n=1}^{N} \underline{y}^n \bar{f}^n + \sum_{n=L+1}^{N} \underline{y}^n \underline{f}^n}{\sum_{n=1}^{N} \bar{f}^n + \sum_{n=L+1}^{N} \underline{f}^n}. \tag{9}$$

Here by using the Karnik-Mendel (KM) algorithms [22], the switching points R and L are obtained. 4. At last, by converting the TR output sets, the mean operation of final crisp output is computed as:

$$y = \frac{y_l + y_r}{2}. \tag{10}$$

3 Robot kinematics and dynamics

3.1 Kinematics analysis

The cable-driven robots have a closed kinematic chain mechanism due to the movement structure. In Figure 2, the kinematics structure of a conventional cable-driven parallel robot with n cables is shown. In this figure, l_i is the vector along ith cable and the length of the cables are equal. B_i and A_i represent attachment points and S_i defines the unit vector along the ith cable on the base and the end-effector. Clearly, b_i is a constant vector in the end-effector frame F_e and a_i denotes the constant vector in the base frame F_o. The point P represents the origin of the end-effector that is utilized to specify the end-effector position vector. According to Figure 2, the end-effector position vector is expressed as follows:

$$p = a_i + l_i - b_i \qquad (i = 1, 2, ..., n), \tag{11}$$

here vectors are shown in the frame F_o and it is obtained that:

$$l_i^2 = [p - a_i + b_i]^T.[p - a_i + b_i]. \tag{12}$$

By differentiating the above equation and performing some simplifications, Eq.12 is obtained within matrix form as:

$$\dot{L} = Jt, \tag{13}$$

where

$$J = \begin{bmatrix} S_1 & S_2 & \dots & S_n \\ b_1 \times S_1 & b_2 \times S_2 & \dots & b_n \times S_n \end{bmatrix}^T. \tag{14}$$

In which $t = [\dot{p}^T, \omega^T]^T = [\dot{p}_x, \dot{p}_y, \dot{p}_z, \omega_x, \omega_y, \omega_z]^T$ represents the end-effector twist,J shows the Jacobian matrix, $\dot{p}$ denotes the velocity vector of the point p, ω shows the end-effector angular velocity and $\dot{L} = [\dot{l}_1, \dot{l}_1, ..., \dot{l}_n]^T$ is the velocity vector in the cable length space.

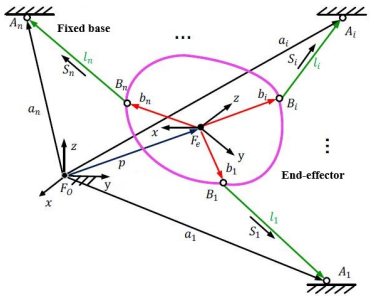


Figure 2: The kinematic schematic of a cable-driven parallel robot

3.2 Dynamic analysis

The dynamic model of a planar cable-driven parallel robot with rigid cable by considering actuator dynamic is obtained as follows [15]:

$$M_{eq}(X)\ddot{X} + C_{eq}(X,\dot{X})\dot{X} + N_{eq}(X,\dot{X}) + \tau_d = J^T u, \tag{15}$$

where

$$\begin{aligned} M_{eq}(X) &= rM(X) + r^{-1}J^T I_m J + \Delta M_{eq}, \\ C_{eq}(X,\dot{X}) &= rC(X,\dot{X}) + r^{-1}J^T I_m \dot{J} + \Delta C_{eq}, \\ N_{eq}(X,X) &= rG(X) + r^{-1}J^T I_m \dot{J}\dot{X} + r^{-1}J^T DJ\dot{X} + \Delta N_{eq}, \\ \tau_d &= T_d + F_d\dot{X} + F_s(\dot{X}). \end{aligned} \tag{16}$$

where $X \in R^6$ is the coordinates vector, I_m denotes the diagonal matrix of actuator inertias, $M(X)$ denotes the inertia matrix, $C(X,\dot{X})$ shows the Coriolis terms, $G(X)$ is the gravitational terms, u represents the input torque and r denotes the pulleys radius. τ_d represents the external load disturbance, F_d is the matrix of viscous fiction, F_s is the coulomb friction term and T_d shows the vector of disturbances. In the above equation, $\triangle Meq$, $\triangle Ceq$ and $\triangle Neq$ represent different parametric uncertainties in the inertia matrix of robots and actuators, geometric structure of robots such as pulleys and gravitational and Coriolis effects. J represents the system Jacobian matrix that relates X to the cable length derivative vector by: $L = J\dot{X}$. Eq.15 can be rewritten as:

$$\ddot{X} = (M_{eq}^{-1}C_{eq})\dot{X} - M_{eq}^{-1}N_{eq} - M_{eq}^{-1}\tau_d + M_{eq}^{-1}J^T u, \tag{17}$$

Eq.17 can be represented as follows:

$$\ddot{X} = D\dot{X} - EN_{eq} - d(t) + FJ^T u, \tag{18}$$

where

$$D = M_{eq}^{-1}C_{eq}, \qquad E = F = M_{eq}^{-1}, \qquad d(t) = M_{eq}^{-1}\tau_d. \tag{19}$$

Note that $d(t)$ is resulted from the uncertain term τ_d. Also, $\triangle D$,$\triangle E$, and $\triangle F$ denote the uncertain terms due to $\triangle Meq$, $\triangle Ceq$ and $\triangle Neq$. The above uncertainties are considered bounded as follows:

$$\begin{cases} \Delta D_l \le |\Delta D| \le \Delta D_h, \\ \Delta F_l \le |\Delta F| \le \Delta F_h, \\ \Delta E_l \le |\Delta E| \le \Delta E_h, \end{cases} \tag{20}$$

where h and l represent the upper and lower values, respectively.

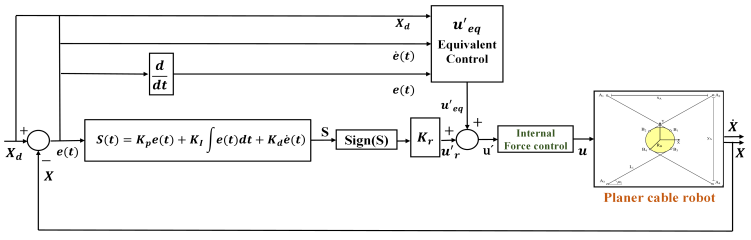


Figure 3: The Block diagram of the sliding mode controller for CDPR

4 Controller design for CDPR

4.1 Sliding mode control

As shown in Figure 3, the sliding proportional-integral-derivative PID surface is defined as:

$$S(t) = K_p e(t) + K_I \int e(t)dt + K_d \dot{e}(t), \tag{21}$$

where $e(t) = X_d - X$ is the tracking error and X_d is the desired position, K_I is the positive integral gain matrix, K_p is the positive proportional gain matrix and K_d is the positive derivative gain matrix that obtained as follows:

$$\begin{cases} K_d = diag(k_{d_1}, k_{d_2}, k_{d3}), \\ K_p = diag(k_{p_1}, k_{p_2}, k_{p3}), \\ K_I = diag(k_{I_1}, k_{I_2}, k_{I3}). \end{cases} \tag{22}$$

Now, by obtaining the derivative of sliding surface and using the Eq.20 , it can be concluded that:

$$\dot{S}(t) = K_p \dot{e}(t) + K_I e(t) + K_d \ddot{X}_d + K_d[(D + \Delta D)\dot{X} - (E + \Delta E)N - (F + \Delta F)J^T u + d(t)]. \tag{23}$$

Now, the control law is defined as:

$$u = u' + rQ, \tag{24}$$

where

$$u' = u'_{eq} + u'_r. \tag{25}$$

In Eq.24, the term Q spans the null space of $\hat{J}^T$ that satisfies $\hat{J}^T Q = 0$. The vector Q is utilized to ensure that all cables stay in tension all over the workspace. In this paper, the motion of the robot is within the wrench-closure workspace and to hold the cables in tension all over the workspace, positive internal forces should be generated Figure 3. Now to evaluate the equivalent control (u'_{eq}), Eq.21 is taken zero without considering the disturbances and the uncertainties. So, the equivalent control is obtained as:

$$u'_{eq} = J^{\dagger}(K_d F)^{-1}[K_p \dot{e}(t) + K_I e(t) + K_d \ddot{X}_d + K_d D\dot{X} + K_d EN], \tag{26}$$

$$u'_r = J^{\dagger} u'_{sw}, \tag{27}$$

where

$$J^{\dagger} = J(J^{\dagger} J)^{-1}. \tag{28}$$

Theorem 4.1. *By applying the control law Eq.24 with the sliding surface Eq.21 to the planar cable-driven parallel robot represented in Eq.15, the closed-loop system is asymptotically stable.*

Proof. The Lyapunov function candidate is chosen as follows:

$$V = \frac{1}{2} S^T S, \tag{29}$$

with V(t) > 0 and V(0) = 0. In order to prove the stability, the derivative of the function V must be negative-definite as follows:

$$\dot{V} = S^T \dot{S} < 0. \tag{30}$$

To include the switching condition, the equivalent control given in Eq.26 is compensated by the u'_r term. To obtain this term, Eq.30 is rewritten as:

$$\dot{V} = S^T(K_p \dot{e} + K_I e + K_d \ddot{e}) = S\left\{K_p \dot{e} + K_I e + K_d[\ddot{X}_d - X]\right\}. \tag{31}$$

By replacing into Eq.31, we have:

$$\dot{V} = S^T\left\{K_p \dot{e} + K_I e + K_d[\ddot{X}_d + (D + \Delta D)\dot{X} + (E + \Delta E)N - (F + \Delta F)J^T(u' + rQ) + d(t)]\right\}. \tag{32}$$

Replacing Eq.25 into Eq.32 results in:

$$\begin{aligned}\dot{V} = S^T \Big\{ K_p\dot{e} + K_I e + K_d\ddot{X}_d + K_d D\dot{X} + K_d\Delta D\dot{X} + K_d EN + K_d\Delta EN + K_d d(t) \Big\} - \\ S^T K_d(F+\Delta F)J^T[J^\dagger((K_dF))^{-1}[K_p\dot{e} + K_I e + K_d\ddot{X}_d + K_d D\dot{X} + K_d EN] + u'_{sw}) + rQ].\end{aligned} \tag{33}$$

Simplifying Eq.33, one can obtain:

$$\begin{aligned}\dot{V} = S^T \Big\{ K_d[\Delta D - F^{-1}D\Delta F)\dot{X} + (\Delta E - F^{-1}E\Delta F)N + d(t)] - F^{-1}E\Delta F(K_p\dot{e} + K_I e + K_d\ddot{X}_d) \Big\} \\ -S^T K_d(F+\Delta F)J^T J^\dagger u'_{sw} - S^T K_d(F+\Delta F)J^T rQ],\end{aligned} \tag{34}$$

which can be written as follows:

$$\begin{aligned}\dot{V} \leq S^T \Big\{ K_d[\left|\Delta D - F^{-1}D\Delta F\right|] \left|\dot{X}\right| + \left|(\Delta E - F^{-1}E\Delta F)\right| |N| + |d(t)|] - \left|F^{-1}\Delta F\right| (K_p |\dot{e}| + K_I |e| + K_d \left|\ddot{X}_d\right|) \Big\} \\ -S^T K_d |(F+\Delta F| J^T J^\dagger u'_{sw} - S^T K_d |(F+\Delta F)| \left|J^T\right| (r |Q|).\end{aligned} \tag{35}$$

To have $S\dot{S} \leq 0$, the reaching control law can be selected as follows:

$$\begin{aligned}u'_{sw} = \mathrm{sgn}(S)[K_d(F+\Delta F_l)J^T J^\dagger]^{-1}\{\left|\Delta D_h - F^{-1}\Delta F_l\right| \left|\dot{X}\right| + \\ \left|(\Delta E_h - F^{-1}E\Delta F_l |N| + K_d |d(t)|\right| - \left|F^{-1}\Delta F_h\right| (K_p |\dot{e}| + K_I |e| + K_d \left|\ddot{X}_d\right|) - |F+\Delta F_l| \left|J^T\right| (r |Q|)\}.\end{aligned} \tag{36}$$

It is obvious that by substituting the obtained reaching controller in Eq.36 into the Eq.35, the condition $\dot{V} = S^T\dot{S} \leq 0$ is satisfied and the closed loop control system approaches towards the stable region. The reaching control term can be expressed as:

$$u'_{sw} = K_r \mathrm{sgn}(S), \tag{37}$$

$$K_r = diag(k_{r_1}, ..., k_{r_n}), \tag{38}$$

where $sgn(.)$ is a sign function and K_r is the reaching control gain which depends on the upper bound of uncertainties. Due to the sign function in the reaching control, selecting high gain values leads to the chattering phenomenon that is a destructive effect on the system, whereas the system might to be unstable if small gain value is chosen. □

4.2 Interval type-2 fuzzy sliding mode control

Recently the chattering phenomenon has been tackled by utilizing the fuzzy logic system to specify the appropriate switching control law. It should be noted that by specifying the proper switching control law, the chattering effect is reduced without loss of robustness. The configuration of the developed interval type-2 fuzzy sliding mode control (IT-2FSMC) scheme is shown in Figure 4. The proposed interval type-2 fuzzy controller has two inputs and one output and the fuzzy inference engine is the Mamdani method. The reaching control law can be suggested as follows:

$$u'_{sw} = K_f U_f(t), \tag{39}$$

where $U_f(t)$ denotes the FSMC output determined by the normalized S and $\dot{S}$, also K_f shows the output variable normalization factor. The input linguistic variables are mapped to the output linguistic variable by the fuzzy control rules as:

$$U_f(t) = FSMC(S, \dot{S}), \tag{40}$$

where $U_f(t) = FSMC(S, \dot{S})$ shows the function of fuzzy linguistic decision scheme. The input membership functions and those of output have been displayed in Figure 5, respectively. They are separated into seven fuzzy parts expressed as PB (Positive Big), PM (Positive Medium), PS (Positive Small), Z (Zero), NM (Negative Medium), NS (Negative Small), and NB (Negative Big). The designed fuzzy rule table is shown in table1. A fuzzy rule form for IT2FSMC has been generated as:

$$R^{(l)} :: \text{If} \quad S(t) \quad \text{is} \quad A^l_{11} \quad \text{and} \quad \dot{S}(t) \quad is \quad A^l_{12} \quad \text{, then} \quad U_f(t) \quad is \quad B^l_1 \qquad l = 1, ..., m, \tag{41}$$

where A^l_{11} and A^l_{12} are the fuzzy input sets and B^l is the fuzzy output set. Totally, the control law of IT-2FSMC can be expressed as:

$$u' = u'_{eq} + u'_{sw} = u'_{eq} + K_f U_f(t), \tag{42}$$

$$u' = u'_{eq} + K_f IT2FSMC(S, \dot{S}). \tag{43}$$

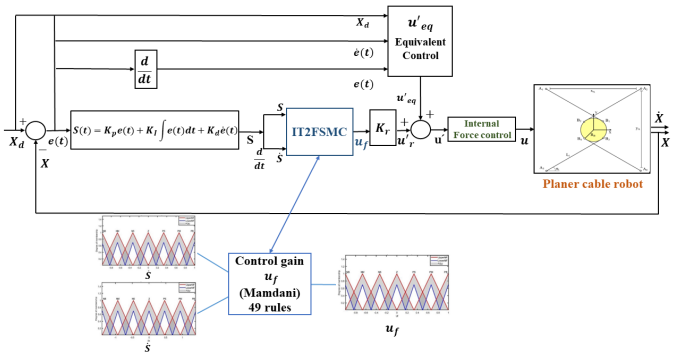


Figure 4: The Block diagram of the IT-2FSMC for CDPR

Table 1: The rules for the reaching control law of the IT-2FSMC

U_f	S						
dS	NB	NM	NS	Z	PS	PM	PB
NB	NB	NB	NB	NB	NM	NS	Z
NB	NB	NB	NB	NM	NS	Z	PS
NS	NB	NB	NM	NS	Z	PS	PM
Z	NB	NM	NS	Z	PS	PM	PB
PS	NM	NS	Z	PS	PM	PB	PB
PM	NS	Z	PS	PM	PB	PB	PB
PB	Z	PS	PM	PB	PB	PB	PB

Theorem 4.2. *The asymptotically stability of CDPR according to the system dynamics expressed in Eq.24 with the equivalent control part in Eq.25 and Eq.42 is proved.*

Proof. The Lyapunov function candidate is chosen as follows:

$$V = \frac{1}{2} S^T S, \tag{44}$$

where $V(t) > 0$ and $V(0) = 0$. The sufficient condition that should be satisfied for the stability is $\dot{V} < 0$. Taking the derivative of the function V yields:

$$\dot{V} = S\dot{S} < 0. \tag{45}$$

Eq.18 can be rearranged as:

$$\ddot{X} = -D\dot{X} - EN + FJ^T u - \Delta D\dot{X} - \Delta EN - d(t) + \Delta FJ^T u, \tag{46}$$

where

$$\ddot{X} = -D\dot{X} - EN + FJ^T u - L(t),$$

$$L(t) = \Delta D\dot{X} + \Delta EN + d(t) - \Delta FJ^T u. \tag{47}$$

So, it is obtained that:

$$\dot{V} = S^T\{K_p\dot{e} + K_I e + K_d\ddot{X}_d + K_d[D\dot{X} + EN - FJ^T(u' + rQ) + L(t)]\}. \tag{48}$$

By replacing Eq.42 into Eq.48, we have:

$$\dot{V} = S^T\{K_p\dot{e} + K_I e + K_d\ddot{X}_d + K_d[D\dot{X} + EN - FJ^T(u'_{eq} + u'_{sw} + rQ) + L(t)]\}. \tag{49}$$

According to the obtained equivalent control in Eq.26, we have:

$$\begin{aligned}\dot{V} = S^T\{&K_p\dot{e} + K_I e + K_d[\ddot{X}_d + K_d D\dot{X} + EN \\ &-FJ^T[J^\dagger((K_d F)^{-1}[K_p\dot{e}(t) + K_I e(t) + K_d\ddot{X}_d + K_d D\dot{X} + K_d EN] + u'_{sw}) + rQ] + L(t)]\}.\end{aligned} \tag{50}$$

Table 2: Rule table for reaching control law of AFSMC

K_f	e						
de	NB	NM	NS	Z	PS	PM	PB
NB	M	S	VS	VVS	VS	S	M
NB	B	M	S	VS	S	M	B
NS	VB	B	M	S	M	B	VB
Z	VVB	VB	B	M	B	VB	VVB
PS	VB	B	M	S	M	B	VB
PM	B	M	S	VS	S	M	B
PB	M	S	VS	VVS	VS	S	M

Simplifying Eq.49 results in:

$$\begin{aligned}&\dot{V} = S^T\{K_p\dot{e} + K_I e + K_d[\ddot{X}_d + K_d D\dot{X} + EN] \\ &-K_d F(J^T[J^{\dagger}((K_d F)^{-1}[K_p\dot{e}(t) + K_I e(t) + K_d\ddot{X}_d + K_d D\dot{X} + K_d EN] + u'_{sw}) + rQ) + L(t)]\}.\end{aligned} \tag{51}$$

So, it is satisfied that:

$$\dot{V} = S^T\dot{S} = S^T\{K_d L(t) - u'_{sw} - rQ\} = S^T\{K_d L(t) - K_f IT2FSMC(S,\dot{S}) - rQ\}. \tag{52}$$

Generally, the normalization of the output fuzzy sets is performed in $[-1,1]$, therefore:

$$\left|u_f = K_f IT2FSMC(S,\dot{S}) \leq 1\right|. \tag{53}$$

And according to Eq.42 and Eq.43, it can be concluded:

$$\dot{V} = S^T\dot{S} \leq K_d\left|L(t)\right|\left|S\right| - K_f\left|S\right| - rQ\left|S\right|. \tag{54}$$

Simplifying relation Eq.54 results in:

$$\dot{V} \leq \{K_d\left|L(t)\right| - K_f - rQ\}\left|S\right|. \tag{55}$$

Therefore, by choosing $K_d\left|L(t)\right| < (K_f + rQ)$, $\dot{V} = S^T\dot{S} \leq 0$ is satisfied and the closed-loop stability is proved. □

4.3 Adaptive interval Type-2 fuzzy sliding mode control

In this section, design of an adaptive interval type-2 fuzzy sliding mode control (AIT-2FSMC) for the CDPR is described. The proposed controller is designed by including an adaptive control gain to the interval type-2 fuzzy sliding mode controller. Figure 6 shows the block diagram of the suggested controller. The mechanism of the adaptive fuzzy system is employed to adaptively tune the reaching control gain K_f and improve the controller performance. The proposed fuzzy controller rules are generated by the linguistic variables. The membership functions of the input and

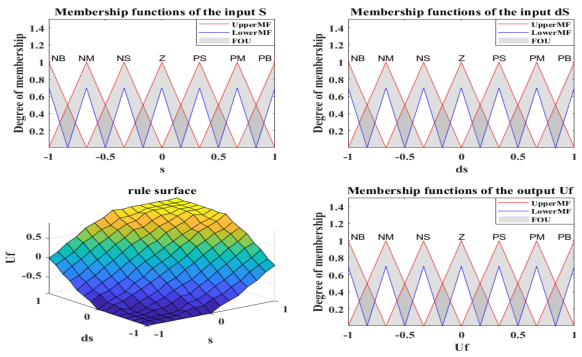


Figure 5: The membership functions of inputs and output and rule surface of IT-2FSMC

output variables are selected as triangular types that shown in Figure 7. Rule table for reaching control law of AFSMC is show in table2.The defined fuzzy variables for the supervisory fuzzy control rules are $(e, \dot{e}) = \{$PM (Positive Medium), PB (Positive Big), PS (Positive Small), Z(Zero), NM (Negative Medium), NB (Negative Big), NS (Negative Small), (Kf) = VVB (Very Very Big), VB (Very Big), B (Big), M (Medium), VVS (Very Very Small), VS (Very Small),S(Small)$\}$. A fuzzy rule form for AIT2FSMC has been generated as:

$$R^{(l)} :: \text{If} \quad e(t) \quad \text{is} \quad A_{11}^{l} \quad \text{and} \quad \dot{e}(t) \quad \text{is} \quad A_{12}^{l} \quad \text{, then} \quad K_f(t) \quad \text{is} \quad B_1^{l} \qquad l = 1, ..., m. \tag{56}$$

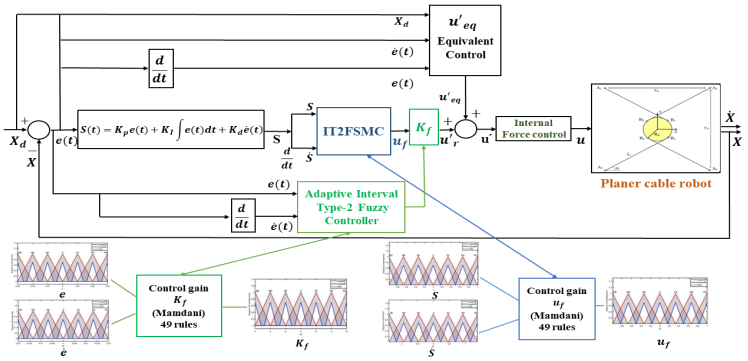


Figure 6: The Block diagram of the AIT-2FSMC for CDPR

4.4 Supervisory adaptive interval Type-2 fuzzy sliding mode control with optimal fuzzy PID sliding surface

In this section, to have better tracking of reference trajectories, a supervisory interval type-2 fuzzy inference system is used for online tuning of the PID sliding surface gains that shows more advantageous compared to the constant gains. The control structure of the suggested controller is shown in Figure 8. In this figure, the interval type-2 fuzzy system is utilized for tuning the u_f signal such as interval type-2 fuzzy sliding mode controller, and also an interval type-2 fuzzy system is considered for tuning the K_f such as the adaptive interval type-2 fuzzy sliding mode controller. K_i,K_d and K_p are the PID sliding surface gains which are tuned online by an interval the derivative of tracking error $\dot{e}$. So, the sliding surface of the controller becomes an intelligent fuzzy sliding surface.The grasshopper optimization algorithm is used to optimize the parameters of the input and output membership functions of the fuzzy sliding surface. The inputs of the designed fuzzy system for the sliding surface are the tracking error (e) and the derivative of the tracking error $\dot{e}$. The outputs of the fuzzy system are the normalized values K_{pp} ,K_{dd} and α which are tuned online ,and then by using equations Eq.57to Eq.59 , the values of the fuzzy PID sliding surface gains are obtained as:

$$K_{dd} = \frac{K_d - K_{d.\min}}{K_{d.\max} - K_{d.\min}}, \tag{57}$$

$$K_i = \frac{K_p^2}{\alpha K_d}, \tag{58}$$

$$K_{pp} = \frac{K_p - K_{p.\min}}{K_{p.\max} - K_{p.\min}}. \tag{59}$$

where $K_{d.\min}$,$K_{d.\max}$,and $K_{p.\max}$ are constant gains,K_{pp} ,K_{dd} and α are output of the interval type-2 fuzzy controller, also K_p,K_i and K_d are tuned gains of the sliding surface. In the following, the Grasshopper Optimization Algorithm (GOA) is introduced in order to optimize the interval type-2 fuzzy sliding surface gains. In other words, by using the GOA, the input and output membership functions of the interval type-2 fuzzy sliding surface are put in the optimal value and best position. Now it is better to give a concise introduction of the grasshopper optimization algorithm and how it works. The GOA is the population-based algorithm and in the category of swarmed intelligence optimization methods which has attracted a lot of attention in recent years. To optimize the calculations of GOA, the grasshopper's swarming behaviors are mimicking. The life cycle of the grasshoppers can be represented in Figure 9a. The GOA has a specific adaptive structure that supplies evenly balanced exploitation and exploration and also fast convergence

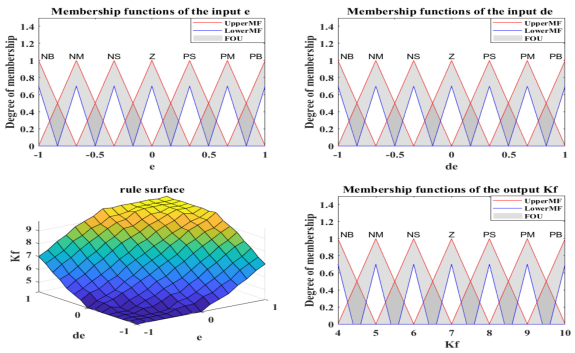


Figure 7: The membership functions of inputs and output and rule surface of AIT-2FSMC

speed with high exploration is provided. The swarming behavior of the grasshoppers is affected by the wind blow, social interaction ,and gravitational force. The i_{th} grasshopper's position in the swarming behavior is mathematically modeled which expressed as:

$$X_i = S_i + W_i + G_i, \tag{60}$$

where X_i denotes the i_{th} grasshopper's position, S_i shows the social interaction of the i_{th} grasshopper, and W_i denotes the wind advection effects ,and the gravitational force on the i_{th} grasshopper shows by G_i. The social interaction of grasshoppers with themselves is an important part of the grasshopper's position which can be obtained as:

$$S_i = \sum_{\substack{j=1 \\ j \neq i}}^{N} s(d_{ij})\widehat{d}_{ij}, \tag{61}$$

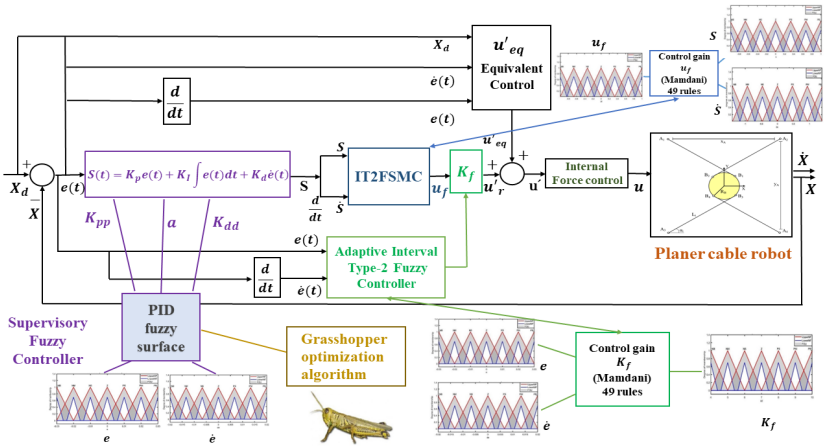


Figure 8: The Block diagram of Supervisory Adaptive Interval Type-2 Fuzzy Sliding mode control with Optimal GOA based Fuzzy PID Sliding Surface for CDPR

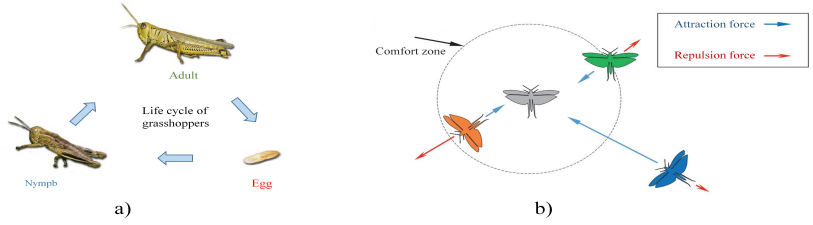


Figure 9: (a) The life cycle of grasshoppers (b) Primary corrective interactions between grasshoppers in a swarm

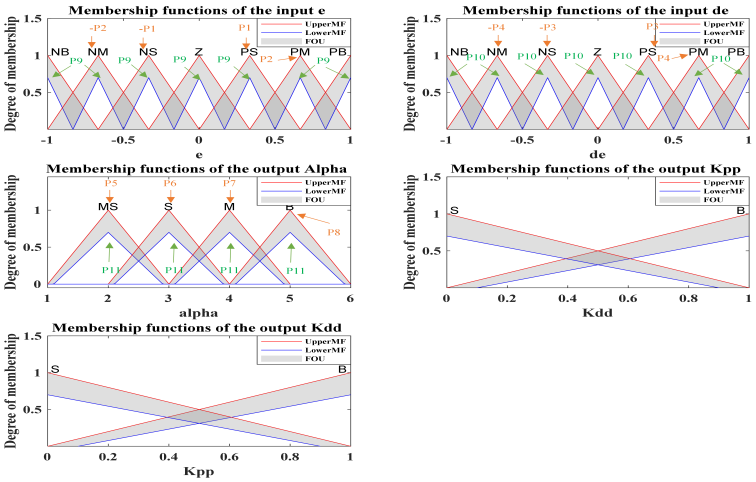


Figure 10: The membership functions of the inputs and output of the SAIT-2FSMC before optimization

$$d_{ij} = |x_j - x_i| . \tag{62}$$

Here s denotes a function to express the power of the social force represented as Eq.63,d_{ij} shows the distance between the i_{th} and j_{th} grasshoppers, and $\widehat{d}_{ij} = \frac{x_j - x_i}{d_{ij}}$ is a unit vector from the i_{th} grasshopper to the j_{th} grasshopper:

$$s(r) = fe^{\frac{-r}{l}} - e^{-r}, \tag{63}$$

where l denotes the attractive length scale and f shows the attraction intensity. Interactions between grasshoppers in a swarm and also the comfort zone, repulsion force, and attraction force are indicated in Figure 9b. The W component in Eq.60 is computed as:

$$W_i = u\widehat{e}_w, \tag{64}$$

where $\widehat{e}_w$ denotes the unit vector in the wind direction, and u shows the constant drift. The G component in Eq.60 is computed as:

$$G_i = -g\widehat{e}_g, \tag{65}$$

where $\widehat{e}_g$ denotes the unity vector towards the earth centre, and g indicates the gravitational constant. Eq.61 can be rewritten as follows:

$$X_i = \sum_{\substack{j=1 \\ j \neq i}}^{N} s(|x_j - x_i|) \frac{x_j - x_i}{d_{ij}} - g\widehat{e}_g + u\widehat{e}_w, \tag{66}$$

where N denotes the grasshoppers' number. Due to the fast attaining of grasshoppers to the comfort zone, the mathematical model expressed in Eq.66 should be modified to show the exploitation and exploration in various stages of the optimization and achieve the global optimum by the accurate approximation. The suggested mathematical model can be described as:

$$X_i^d = c\Big(\sum_{\substack{j=1 \\ j \neq i}}^{N} c\frac{ub_d - lb_d}{2} s\big(\big|x_j^d - x_i^d\big|\big) \frac{x_j - x_i}{d_{ij}}\Big) + \widehat{T}_d, \tag{67}$$

$$C = C_{\max} - l\frac{C_{\max} - C_{\min}}{L}, \tag{68}$$

where lb_d is the lower bound and ub_d is the upper bound in the D_{th} dimension, $\widehat{T}_d$ denotes the global best of k_{th} variable (best solution found), C indicates the decreasing factor to shrink the attraction zone, repulsion zone and comfort zone. Also, C_{min} and C_{max} show the minimum and maximum values of C, respectively, l denotes the current iteration and L indicates the maximum number of iterations.

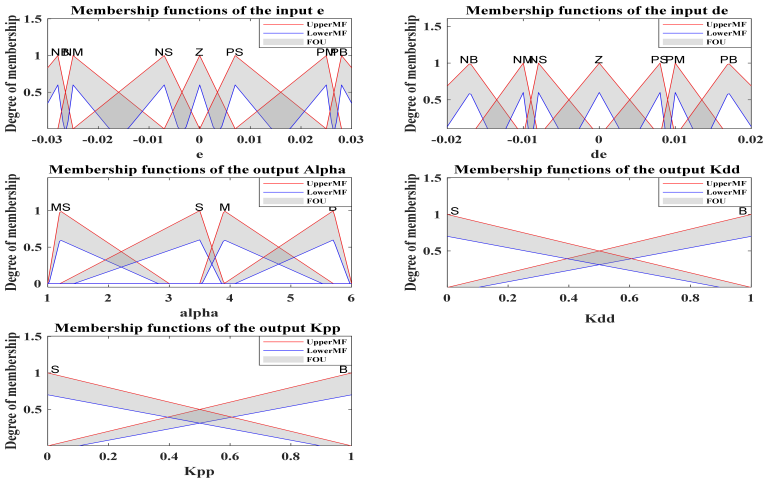


Figure 11: The membership functions of the inputs and output of the SAIT-2FSMC after optimization

In this paper, the values 0.00001 and 1 are taken for the C_{min} and C_{max} , respectively. In Figure 10, $P_1, ..., P_{11}$ are the fuzzy membership parameters that optimized with the GWO according to the cost function represented in Eq. (70). GWO chooses the appropriate values for the $P_1, ..., P_{11}$ to minimize the cost function. The cost function is generally offered as a function of tracking errors (x, y, φ) as follows:

$$f = \sqrt{(e_x^2 + e_y^2 + e_\varphi^2)}. \tag{69}$$

In the current work, the symmetry feature of the membership functions is used to prevent the definition of the new parameters and so decrease the calculations. All of the parameters that have been selected to be optimized by the GOA are specified in Figure 10. $P1$ and $P2$ are the second parameters of the fifth and sixth upper membership functions respectively.Now by using the symmetry feature of the membership functions, $-P1$ and $-P2$ are defined as the second parameters of the second and third upper membership functions, respectively, also, $-P3$ and $-P4$ are similarly defined. $P5$, $P6$, $P7$, and $P8$ are the second parameters of the first to fourth upper membership functions of the alpha output, respectively. $P9$, $P10$ and $P11$ are defined as the lower scales of the fuzzy parameters, respectively. To optimize the parameters of the membership functions by using the GOA, the optimal membership functions of the fuzzy sliding surface are obtained as shown in Figure 11. A fuzzy rule form of the proposed interval type-2 fuzzy sliding surface controller is represented as:

$$R^{(l)} :: \text{If } e(t) \text{ is } A_{l1}^l \text{ and } \dot{e}(t) \text{ is } A_{l2}^l \text{ ,then } K_{pp}(t) \text{ is } B^l \text{ , } K_{dd}(t) \text{ is } S^l \text{ , } \alpha^l \text{ is } 2 \quad l = 1, ..., m. \tag{70}$$

Table 3 to table 5 represent the rules for tuning the K_{pp} ,K_{dd} and $Alpha$ respectively.

Table 3: Rules considered for K_{pp}

K_{pp}	de						
e	NB	NM	NS	ZO	PS	PM	PB
NB	B	B	B	B	B	B	B
NB	S	B	B	B	B	B	S
NS	S	S	B	B	B	S	S
ZO	S	S	S	B	S	S	S
S	S	B	B	B	B	S	S
PM	S	B	B	B	B	B	S
PB	B	B	B	B	B	B	B

Table 4: Rules considered for K_{dd}

K_{dd}	de						
e	NB	NM	NS	ZO	PS	PM	PB
NB	S	S	S	S	S	S	S
NB	B	B	S	S	S	B	B
NS	B	B	B	S	B	B	B
ZO	B	B	B	B	B	B	B
S	B	B	B	S	B	B	B
PM	B	B	S	S	S	B	B
PB	S	S	S	S	S	S	S

5 Simulation and results

A fully constrained planar cable-driven parallel robot is considered as denoted in Figure 12a which has been used for investigating the efficacy of the suggested controller. This robot has three degrees of freedom, $P = (x, y, \varphi)$, that

Table 5: Rules considered for *Alpha*

Alpha	de						
e	NB	NM	NS	ZO	PS	PM	PB
NB	2	2	2	2	2	2	2
NB	3	3	2	2	2	3	3
NS	4	3	3	2	3	3	4
ZO	5	4	3	3	3	4	5
S	4	3	3	2	3	3	4
PM	3	3	2	2	2	3	3
PB	2	2	2	2	2	2	2

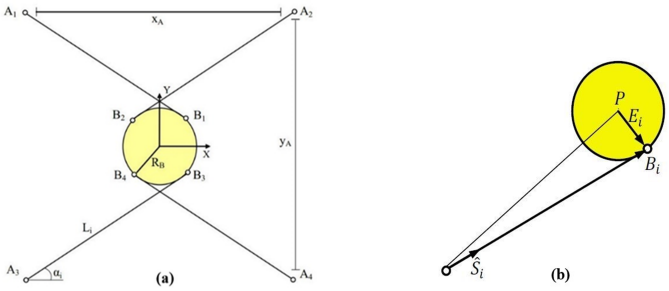


Figure 12: a. The schematics of the planar cable robot mechanism b. Vector definitions for Jacobian derivation

shows the position and orientation of the center of mass of the end-effector and also the robot has one degree of actuator redundancy. The structural properties and dynamic parameters of the considered planar robot is shown in table 6. In Figure 12b, B_i shows the points of connection of the cables on the end-effector and A_i shows the fixed base points of the cables. Also y_A and x_A are the width and length of the rectangle and the actuators jointed on its vertices. In the conducted simulation, $x_A = 2 \pm 0.2m$, $y_A = 2 \pm 0.2m$ are considered as uncertain parameters ,and $R_B = 0.15m$, $K_d = diag([2, 2, 2])$, $K_i = diag([2.5, 2.5, 2.5])$,and $K_p = diag([3, 3, 3])$. The following assumptions are considered for the robot planar motion dynamics:

$$M = diag(m, m, I_z) \quad , \quad C(x, \dot{x}) = 0, \tag{71}$$

where Iz is the moment of inertia and m shows the mass of the end-effector. According to the E_i, S_i vectors denoted in Figure 12b, the non-square Jacobian matrix of the planer cable robot is represented as:

$$J = \begin{pmatrix} S_{1x} & S_{1y} & E_{1x}S_{1y} - E_{1y}S_{1x} \\ S_{2x} & S_{2y} & E_{2x}S_{2y} - E_{2y}S_{2x} \\ S_{3x} & S_{3y} & E_{3x}S_{3y} - E_{3y}S_{3x} \\ S_{4x} & S_{4y} & E_{4x}S_{4y} - E_{4y}S_{4x} \end{pmatrix}. \tag{72}$$

Also, the following reference trajectories are considered:

$$x_d = 0.4 + 2e^{-t} - 2.4e^{\frac{-t}{1.2}}, \tag{73}$$

$$y_d = 0.4 + 2e^{-t} - 2.4e^{\frac{-t}{1.2}}, \tag{74}$$

$$\varphi_d = 0.2\sin(0.2\pi t). \tag{75}$$

The considered uncertainties and disturbances in the simulations are as follows:

$$\begin{cases} \Delta D = 0.035I, & \Delta E = \Delta F = 0.05I, & 0 \le t \le 10 \\ \Delta D = 0.020I, & \Delta E = \Delta F = 0.035I, & 10 \le t \le 20 \\ \Delta D = 0.010I, & \Delta E = \Delta F = 0.020I, & 20 \le t \le 30 \end{cases} \tag{76}$$

$$\begin{cases} \tau_d = 0.15G(x), & 0 \le t \le 10 \\ \tau_d = 0.10G(x), & 10 \le t \le 20 \\ \tau_d = 0.5G(x), & 20 \le t \le 30 \end{cases} \tag{77}$$

Figure 13 shows the tracking reference trajectories for the SMC, IT-2FSMC, and AIT-2FSMC with PID sliding surface, and the developed SAIT-2FSMC with fuzzy PID sliding surface.This figure also shows the results obtained by the controller with type 1 fuzzy structure (FSMC). The tracking error profiles have also been displayed in Figure 14.

The simulation results show that the SAIT-2FSMC with fuzzy PID sliding surface has lower error values which is due to this fact that the PID gains of the sliding surface are adjusted by the proposed supervisory fuzzy gain scheduling method; also, the parameters of the fuzzy MFs are optimally chosen by the GOA. Figure 15 shows the cable tension for control of the CDPR provided by different methods. It is evident in this figure that the chattering amount for the developed method has been reduced to an acceptable level and has a considerable correction compared to the methods that do not have the ability to remove it. In this figure, the production of purely tensile force for different algorithms is confirmed that shows that the control objectives have been met in terms of the structural challenges associated with cable robots. The performance of tracking the desired circular trajectory in the XY plane is shown in Figure 16. The merits and efficacy of the suggested composite controller can be observed in this figure. In table 7, different algorithms have been compared in terms of achievable accuracy, convergence time and the required control effort. In this table, the mean square error (MSE) performance index has been used to provide the efficiency of the mentioned algorithms. The computational load of different algorithms relative to each other is evaluated by the timeit operation in MATLAB. Also, the integral of control effort are intended to show the amount of energy consumed. The results collected in table 7 demonstrate the merits of the developed algorithm compared to the related methods. According to this table, the designed algorithm has relatively more convergence time in comparison to less complex systems (such as type 1 fuzzy systems), but this difference is not significant and so the suggested method can still be used for real applications. Also, due to selection of appropriate parameters in the proposed algorithm, despite its greater complexity, it has an acceptable level of control.

Table 6: The structural properties and dynamic parameters of the planar robot

Parameters	Value	Symbol
The actuator drum radius	$3.5cm$	r
The actuator inertias	$0.6 \pm 0.1kgm^2$	I_m
End-effector mass	$2.5 \pm 0.5kg$	m
End-effector inertia	$0.03 \pm 0.01kgm^2$	I_z

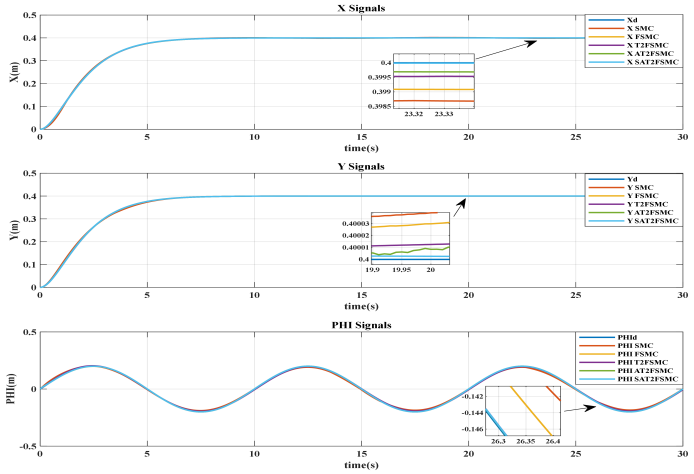


Figure 13: Tracking reference trajectories for different control

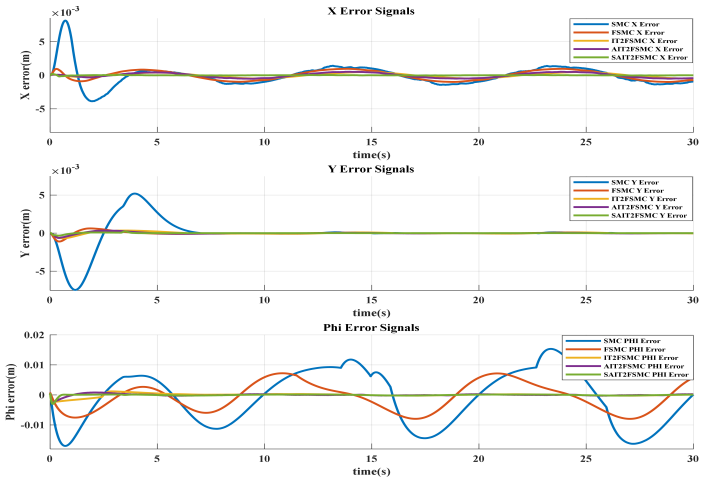


Figure 14: Tracking error for different controllers

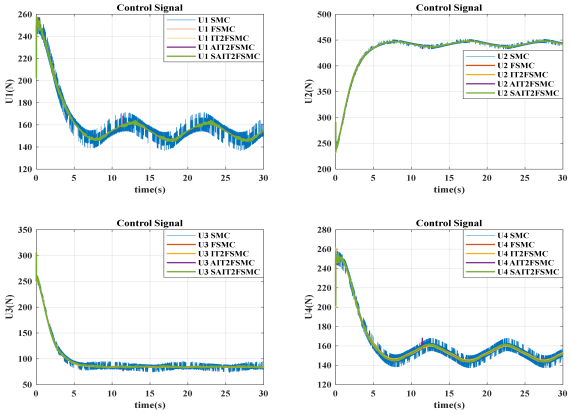


Figure 15: Cables tension for control of CDPR for different controllers

6 Conclusions

Development of an adaptive supervisory fuzzy sliding mode control was considered in this paper that successfully applied for the control of the cable-driven parallel robots. The fuzzy logic system is used to generate the switching control signal to remove the chattering effect, and also an adaptive mechanism is suggested for online tuning of the output gain of the fuzzy sliding mode control.In addition, for reduction of the tracking errors, a fuzzy system was designed as a supervisory controller for online tuning of the PID sliding surface gains. The Grasshopper optimization algorithm is offered for optimization of the membership functions of the fuzzy system. The benefits of the proposed procedure are the reduction of the chattering and system robustness against parameters uncertainties, nonlinearities, and load disturbances. Simulation results show the merits and efficacy of the proposed control method. It was confirmed that the developed algorithm has a lower tracking error compared to similar methods while this performance occurs at an acceptable computational time and with an appropriate energy level. Achieving a performance with a fixed convergence time and assuming no access to the required states of the robot will be considered in future works.

Acknowledgement

The authors thankfully acknowledge the comments and suggestions from the Managing Editor and anonymous referees.This work received no financial support for the research, authorship, and publication of this article.

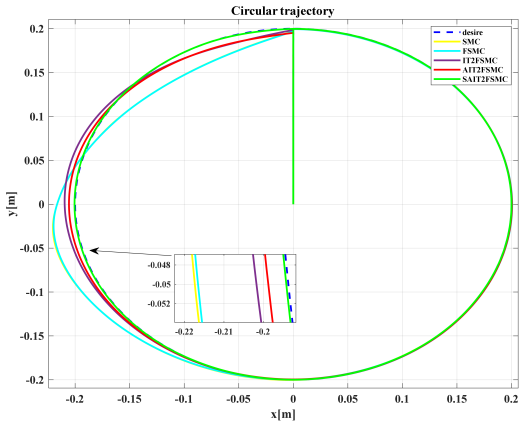


Figure 16: Tracking the desired circular trajectory in the XY plane for different controllers

Table 7: The Performance compared for different methods

	MSE			Run time(S)	Control energy(j)			
Algorithm	e_x	e_y	e_φ	t	u_1	u_2	u_3	u_4
SMC	3.51×10^{-6}	1.49×10^{-6}	8.23×10^{-5}	8.42	4712	9213	2845	4644
FSMC	4.65×10^{-6}	9.23×10^{-7}	9.02×10^{-6}	14.03	4655	8917	2764	4527
IT2FSMC	9.53×10^{-6}	6.75×10^{-7}	3.76×10^{-6}	15.56	4590	8803	2778	4467
AIT2FSMC	7.28×10^{-7}	3.43×10^{-7}	1.25×10^{-6}	16.34	4566	9032	2712	4514
SAIT2FSMC	1.21×10^{-7}	0.56×10^{-7}	9.26×10^{-7}	18.18	4612	9102	2765	4523

References

[1] S. Abdolshah, E. Barjuei, *Linear quadratic optimal controller for cable-driven parallel robots*, Frontiers of Mechanical Engineering, **4** (2015), 344-351.

[2] M. Aghaseyedabdollah, Y. Alaviyan, H. Azmi, A. Yazdizadeh, *Fuzzy fractional order sliding mode controller design for a wind turbine with DFIG*, Iranian Conference on Electrical Engineering, (2021), 637-642.

[3] D. Ayedi, M. Boujelben, C. Rekik, *Hybrid type-2 fuzzy-sliding mode controller for navigation of mobile robot in an environment containing a dynamic target*, Journal of Robotics, **2018** (2018), 1-10.

[4] R. Babaghasabha, M. A. Khosravi, H. D. Taghirad, *Adaptive robust control of fullyconstrained cable driven parallel robots*, Mechatronics, **25** (2015), 27-36.

[5] N. Bakhshinezhad, S. A. Mir Mohammad Sadeghi, A. R. Fathi, H. R. Mohammadi Daniali, *Adaptive particularly tunable fuzzy particle swarm optimization algorithm*, Iranian Journal of Fuzzy Systems, **17** (2020), 65-75.

[6] P. M. Bosscher, *Disturbance robustness measures and wrench feasible workspace generation techniques for cable driven robots*, Georgia Institute of Technology, (2004), URI: http://hdl.handle.net/1853/4875.

[7] R. Bostelman, J. Albus, N. Dagalakis, A. Jacoff, J. Gross , *Applications of the NIST RoboCrane*, In Proceedings of the 5th International Symposium on Robotics and Manufacturing, **5** (1994), 1-9.

[8] M. Carpio, R. Saltaren, J. Viola, C. Calderon, J. Guerra, *Proposal of a decoupled structure of fuzzy PID controllers applied to the position control in a planar CDPR*, Electronics, **10**(6) (2021), 745-766.

[9] N. Doikov, Y. Nesterov, *Minimizing uniformly convex functions by cubic regularization of Newton method*, Journal of Optimization Theory and Applications, **189** (2021), 317-339.

[10] H. R. Fahham, M. Farid, M. Khooran, *Time optimal trajectory tracking of redundant planar cable-suspended robots considering both tension and velocity constraints*, Journal of Dynamic Systems Measurementand Control, **133** (2011), 11-25.

[11] M. Gouttefarde, *Characterizations of fully constrained poses of parallel cabledriven robots*, a review. Proc ASME Int Des Tech Conf, (2008), 3-6.

[12] J. Hwang, Y. Kang, J. Park, D. Kim, *Advanced interval type-2 fuzzy sliding mode control for robot manipulator*, Computational Intelligence and Neuroscience, **2018** (2018), 1-11.

[13] F. Inel, A. Medjbouri, G. Carbone, *A non-linear continuous-time generalized predictive control for a planar cable-driven parallel robot*, In Actuators, Multidisciplinary Digital Publishing Institute, **10** (2021), 97-117.

[14] S. Kawamura, H. Kino, C. Won, *High-speed manipulation by using parallel wire-driven robots*, Robotica, **18**(1) (2000), 13-21.

[15] S. A. Khalilpour, R. Khorrambakht, M. J. Harandi, H. D. Taghirad, P. Cardou, *Robust dynamic sliding mode control of a deployable cable driven robot*, Iranian Conference on Electrical Engineering (ICEE), (2018), 863-868.

[16] M. A. Khosravi, H. D. Taghirad, *Robust PID control of fully-constrained cable driven parallel robots*, Mechatronics, **24**(2) (2014), 87-97.

[17] H. Kino, T. Yahiro, F. Takemura, T. Morizono, *Robust PD control using adaptive compensation for completely restrained parallel-wire driven robots: Translational systems using the minimum number of wires under zero-gravity condition*, IEEE Transactions on Robotics, **23** (2007), 803-812.

[18] E. Laroche, R. Chellal, L. Cuvillon, J. Gangloff, *A preliminary study for H-infty control of parallel cable-driven manipulators*, In Cable-Driven Parallel Robots, (2013), 353-369.

[19] J. Lenarčič, M. Michael, *Advances in robot kinematics motion in man and machine*, Springer Science Business Media, 2010.

[20] W. B. Lim, G. Yang, S. H. Yeo, S. K. Mustafa, *A generic force-closure analysis algorithm for cable-driven parallel manipulators*, Mechanism and Machine Theory, **46** (2011), 1265-1275.

[21] M. Mahmoodabadi, N. Babak, *Fuzzy adaptive robust proportional-integral-derivative control optimized by the multi-objective grasshopper optimization algorithm for a nonlinear quadrotor*, Journal of Vibration and Control, **26** (2020), 1574-1589.

[22] J. Mendel, M. John, R. John, F. Liu, *Interval type-2 fuzzy logic systems made simple*, IEEE Transactions on Fuzzy Systems, **14**(6) (2006), 808-821.

[23] N. Nafia, E. Abdeljalil, H. Ayad, M. Mjahed, *A robust type-2 fuzzy sliding mode controller for disturbed MIMO nonlinear systems with unknown dynamics*, Automatika, **59** (2018), 194-207.

[24] H. Navvabi, A. Markazi, *Hybrid position/force control of stewart manipulator using extended adaptive fuzzy sliding mode controller (E-AFSMC)*, ISA Transactions, **88** (2019), 280-295.

[25] S. R. Oh, S. K. Agrawal, *Generation of feasible set points and control of a cable robot*, IEEE Transactions on Robotics, **22**(3) (2006), 551-558.

[26] M. H. Qais, H. M. Hasanienand, S. Alghuwainem, *Whale optimization algorithm based Sugeno fuzzy logic controller for fault ride through improvement of grid connected variable speed wind generators*, Engineering Applications of Artificial Intelligence, **87** (2020), DOI:10.1016/j.engappai.2019.103328.

[27] M. S. Qureshi, P. Swarnkar, S. Gupta, *A supervisory on-line tuned fuzzy logic-based sliding mode control for robotics an application to surgical robots*, Robotics and Autonomous Systems, **109** (2018), 68-85.

[28] N. Quynh, N. W. Yao, Y. Thi, *A novel robust adaptive control using RFWNNs and backstepping for industrial robot manipulators with dead-zone*, Journal of Intelligent and Robotic Systems, **98** (2020), 679-692.

[29] M. Roopaei, M. Zolghadri, B. Ranjbar, T. Lin, *Synchronization of two different chaotic systems using novel adaptive interval type-2 fuzzy sliding mode control*, Nonlinear Dynamics, **66** (2011), 667-680.

[30] A. S. Shaalan, A. Negar, M. Bardini, M. Sharaf, *Embedded fuzzy sliding mode control for polymer extrusion process*, ISA Transactions, **103** (2020), 237-251.

[31] S. H. Saremi, S. Mirjalili, A. Lewis, *Grasshopper optimisation algorithm: Theory and application*, Advances in Engineering Software, **105** (2017), 30-47.

[32] S. Tripathi, A. Shrivastava, K. Jana, *Self-tuning fuzzy controller for sun-tracker system using Gray Wolf Optimization (GWO) technique*, ISA Transactions, **101** (2020), 50-59.

[33] M. Wei-Lung, D. Yu Shiu, *Precision trajectory tracking on XY motion stage using robust interval Type-2 fuzzy PI sliding mode control method*, International Journal of Precision Engineering and Manufacturing, **21** (2020), 1-22.

[34] D. Zanotto, G. Rosati, S. Minto, A. Rossi, *Sophia-3: A semiadaptive cable-driven rehabilitation device with a tilting working plane*, IEEE Transactions on Robotics, **30** (2014), 974-979.

[35] K. Zheng, H. Youmin, W. Bo, *Intelligent fuzzy sliding mode control for complex robot system with disturbances*, European Journal of Control, **51** (2020), 95-109.